

Original article

Contribution of different shale storage spaces to recovery rate and mechanism of oil mobilization during imbibition

Jianguang Wei^{1,2,3}, Anlun Wang^{1,2,3}, Rui Wang^{1,4}*, Ying Yang^{1,2,3}, Xiaoqing Zhao^{1,2,3}, Xiaofeng Zhou^{1,2,3}

¹State Key Laboratory of Continental Shale Oil, Northeast Petroleum University, Daqing 163318, P. R. China

²Key Laboratory of Continental Shale Hydrocarbon Accumulation and Efficient Development (Northeast Petroleum University), Ministry of Education, Northeast Petroleum University, Daqing 163318, P. R. China

³Institute of Unconventional Oil & Gas, Northeast Petroleum University, Daqing 163318, P. R. China

⁴Exploration and Development Research Institute of Daqing Oilfield Co. Ltd, Daqing 163712, P. R. China

Keywords:

Shale storage space
imbibition
mobilization mechanism
external fluids
nuclear magnetic resonance

Cited as:

Wei, J., Wang, A., Wang, R., Yang, Y., Zhao, X., Zhou, X. Contribution of different shale storage spaces to recovery rate and mechanism of oil mobilization during imbibition. *Capillarity*, 2025, 15(1): 12-24.
<https://doi.org/10.46690/capi.2025.04.03>

Abstract:

The influence of different reservoir spaces in shale reservoirs on imbibition recovery is a hot spot for improving shale oil recovery. However, the research on the influence of different chemical reagents on the recovery factor of different scale pores is limited, and the influence mechanism of shale imbibition recovery factor under the action of different media has not been systematically studied. Therefore, this study takes the Gulong shale oil reservoir as the research object, carries out imbibition experiments combined with nuclear magnetic resonance testing under different injection fluid conditions, quantifies the contribution of shale pores of different scales to imbibition recovery under different injection media conditions, and analyzes the influence of injection media types on imbibition recovery. The results show that the average contribution rate of different types of pores was in the order of interlayer clay (47.6%) > mesoscale pores (32.7%) > small pores (17.3%) > large pores (2.6%). The total imbibition recovery of shale with millimeter-scale sandy laminae was ranked as alkali solution (61.50%) > acid solution (60.92%) > GJ surfactant (39.79%) > distilled water (32.92%) > guanidine gum (30.38%), and the total imbibition recovery of laminated shale was ranked as GJ surfactant (39.1%) > slick water (38.0%) > guanidine gum (34.7%) > distilled water (29.2%).

1. Introduction

Shale oil resources have significant potential and exhibit obvious zoning and differentiation (Zhang et al., 2023b). Shale oil reservoirs in the northern Songliao Basin are abundant and have unique geological characteristics. For these reservoirs, conventional reservoir characteristic studies cannot meet the needs of precise reservoir evaluation (Liu et al., 2019). Controlled by sedimentary conditions, the Songliao Basin

developed different types of shale oil: interbedded type and shale type (Lee et al., 2020). The interbedded type has been developed on a large scale and the interlayer type exploration has achieved breakthroughs, and shale type is currently the main research direction (Ma et al., 2019). Gulong shale has excellent storage performance, with a variety of storage space types and unique pore types and permeability characteristics (Mohagheghian et al., 2020). Nanoscale matrix pores and foliated fractures are the main storage spaces, primarily including

bedding fractures (clay diagenetic fractures and organic matter contraction fractures) and organic/intergranular pores (Naveen et al., 2018; Sakurovs et al., 2018).

The traditional view is that North American marine shale oil is a kind of light oil and condensate oil (Sun et al., 2017; Ratnakar and Dindoruk, 2019; Jiang et al., 2023). In contrast, the overall degree of thermal evolution results in most of the oil being heavier in terms of quality (Roslin et al., 2020; Sun et al., 2023), leading to its low fluidity (Saghandal et al., 2023). However, according to the oil testing data, it has low density, low viscosity, high formation pressure, and strong flowing ability (Sakurovs et al., 2018; Gao et al., 2024). The surface density of the Qijia-Gulong area is generally less than 840 kg/m^3 , and the overall viscosity of formation crude oil is less than $0.8 \text{ mPa}\cdot\text{s}$ (Shelare et al., 2023). The quality of crude oil in Ping 1 well is significantly better than that of conventional crude oil (Tang et al., 2016; Gao et al., 2025a). In addition, the petroleum surpassing effect is significant, with the movable oil index generally exceeding 100 mg/g and ranging from 200 to 400 mg/g in the lower part of the first and second sections (Wang et al., 2022). As the burial depth increases, the movable oil index rises significantly, indicating that the quality of Gulong shale oil is excellent and has great movable potential (Yakasai et al., 2021). Nano-pores are characterized by strong internal solid-liquid interactions and significant confinement effects on the fluid inside them (Sun et al., 2018; Yang et al., 2022). This is mainly characterized as the strong capillary pressure effect (Zhang et al., 2020), which results in significant differences in the fluid properties and bulk phases (Xiao et al., 2022). Many scholars have demonstrated through experimental studies such as nanoscale fluidic chips and differential scanning calorimetry that the bubble point pressure in nanoscale pores is smaller than that in the bulk state (Zhou et al., 2023). As the pore size decreases, the degree of deviation also gradually increases (Zhou et al., 2016; Gao et al., 2025b). However, because of the unconventional characteristics of rocks and the limitations of experimental equipment (i.e., it is difficult to produce underground nanoscale fluidic chips or nanoscale porous media models), conducting phase behavior experimental research is rather challenging (Zhu et al., 2020). With the advancement of computational science, simulation methods have been widely used to compensate for the shortcomings of experiments (Maghzi et al., 2012; Zhong et al., 2019; Zhang et al., 2023a; Zheng et al., 2023; Wei et al., 2024). Among them, data on the transformation of critical properties of pure substances can be obtained through molecular dynamics simulations (Liu et al., 2023b). However, the above methods cannot describe the essence of critical property transformation through state equations (Xiang et al., 2011; Tao et al., 2023). Therefore, researchers are committed to developing equations of state that can describe the nano-confinement effect (Liu et al., 2020b). On the basis of simulation research, some scholars have found that in addition to the experimental understanding (Liu et al., 2021; Chen et al., 2025), the nano-pore confinement effect can promote gas-phase condensation and reduce liquid density and viscosity (Liu et al., 2020a). Nonetheless, current research about the nano-effect on fluid properties and oil and gas mass transfer

mainly focuses on single-phase or two-phase oil and gas (Xu et al., 2023). In addition, existing models are mostly applicable to Eagle Beach and Bakun, making it difficult to accurately describe the phase behavior (Meng et al., 2023). Besides, the Gulong shale reservoir has a multi-scale storage space (Yu et al., 2023), with a large number of micrometer scale bedding fractures and millimeter-scale pressure fractures in addition to the widely distributed nanoscale pores (Meng et al., 2023; Lu et al., 2025). Under the influence of the nano-confinement effect, the distribution of fluid components in multi-scale space exhibits spatial non-uniformity (Liu et al., 2023a), leading to complex changes in fluid properties and interphase mass transfer laws, thereby affecting the supply and production characteristics of oil from matrix pores to fractures in the production process (Liu et al., 2020c, 2023b; Faramarzi et al., 2025). Shale oil reservoirs exhibit unique behaviors and responses to imbibition due to their unique pore structure and complex physicochemical properties. Imbibition refers to the process of fluid passing through solid media under capillary force (Zhao et al., 2022; Zheng et al., 2025). Firstly, as small pores and fractures in shale oil reservoirs provide appropriate channels, crude oil can be extracted through imbibition. This natural imbibition process helps to increase the fluidity (Wang et al., 2025). Secondly, via imbibition, some chemical substances dissolved in the fluid can enter the shale pores, undergo chemical reactions with the rock, and change the pore structure and physical properties. This in turn improves the permeability and porosity of the reservoir, further increasing the oil recovery rate. Besides, the imbibition effect also helps to reduce the residual oil saturation, further tapping into the reservoir's productivity potential. However, imbibition is also affected by fluid properties and environmental factors (Liu et al., 2023c; Yuan et al., 2023).

Therefore, this study takes the Gulong shale oil reservoir as the research object, carries out imbibition experiments combined with Nuclear Magnetic Resonance (NMR) testing under different injection fluid conditions, analyzes the influence of injection media types on imbibition recovery, and quantifies the contribution of shale pores of different scales to imbibition recovery under different injection media conditions.

2. Experimental section

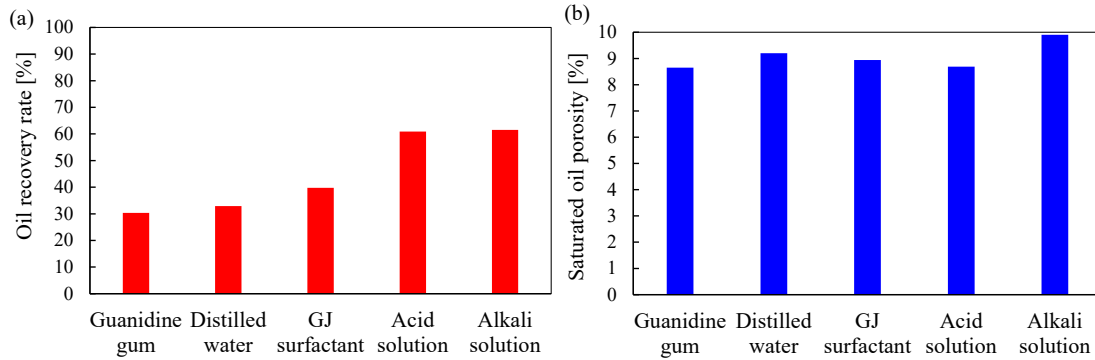
2.1 Materials and equipment

Acid solution: 5 wt.% HF+12 wt.% HCl; Alkaline solution: NaOH (pH = 13); Slick water and guanidine gum; Absorbent solution: GJ surfactant. Two types of composite fracturing fluids were used, which are composed of slick water filtrate and acid solution (5 wt.% HF and 12 wt.% HCl), and absorbent solution (GJ surfactant) and acid (5 wt.% HF and 12 wt.% HCl), respectively. The experimental temperature was $110 \text{ }^\circ\text{C}$, and the experimental pressure was 37 MPa . All related data are presented in Table S1 in Supplementary file.

The instruments are shown in Fig. S1 in Supplementary file.

Table 1. Recovery rate of imbibition under different injection medium conditions.

No.	Injection medium	Core mass (g)	Saturated oil mass (g)	Saturated oil porosity (%)	Recovery rate (%)
4-10-7	Guanidine gum	46.9506	48.2975	8.65	30.38
2-2-4	Distilled water	50.324	51.8565	9.20	32.92
2-3-1	GJ surfactant	48.6861	50.1198	8.94	39.79
1-17-6	Acid solution	70.6995	72.7648	8.69	60.92
4-11-6	Alkali solution	46.1768	47.6955	9.90	61.50

**Fig. 1.** Oil recovery rates and saturated oil porosities: (a) Recovery rates under different chemical agents and (b) saturated oil porosities under different chemical agents.

2.2 Methods

Referring to the NMR testing standards “Laboratory Measurement Specification for NMR Parameters of Rock Samples” SYT 6490-2014 and “Core Analysis Methods” GB/T 29172-2012, specific steps for shale oil permeability and absorption experiments have been developed, as follows:

- 1) Configure external fluids and use filter paper to filter and prepare for the experiment.
- 2) After drying the core at 110 °C for 5 days, weigh it and perform NMR testing.
- 3) Using a gripper, set a confining pressure of 2 MPa, apply 2 days of vacuum, then saturate with shale oil. Keep temperature at constant 110 °C for 1 day.
- 4) At a constant 110 °C, pressurize the core sample to 30/10 MPa to conduct the imbibition experiment. After 15 days, take the core out for NMR.
- 5) Clarify the contributions of shale oil saturation, imbibition recovery rate, different pore sizes, and different types of external fluids to the imbibition recovery rate.

3. Results and discussion

3.1 Experimental results of stimulation

3.1.1 Shale with millimeter-scale sandy laminae

The recovery rates of shale under different injection media conditions calculated based on NMR testing data are presented in Table 1 and Fig. 1. Further comparison of the imbibition recovery rates of guanidine gum, distilled water and GJ surfactant for shale with millimeter-scale sandy laminae reveals that under the conditions of stimulation, the total shale recovery

rate was in the order of GJ surfactant (39.1%) > guanidine gum (34.7%) > distilled water (29.2%).

From Fig. 1, it can be found that after injecting different media into the samples, the sample treated with alkaline solution has the highest recovery rate of 61.50% through imbibition. The next highest stimulation recovery rate results from acid solution at 60.92%. The stimulation recovery rates of samples treated with these two types of media were much higher than those treated with the other three media. The sample treated with guanidine gum had the lowest imbibition recovery rate at only 30.38%, which was 31.12% lower than that of the sample treated with alkaline solution, 32.92% lower than that of distilled water and 39.79% lower than that of GJ surfactant. The saturated oil porosity of the sample treated with alkaline solution was the highest at 9.90%, followed by the sample treated with distilled water. The porosity of saturated oil after acid treatment was the lowest at only 8.69%.

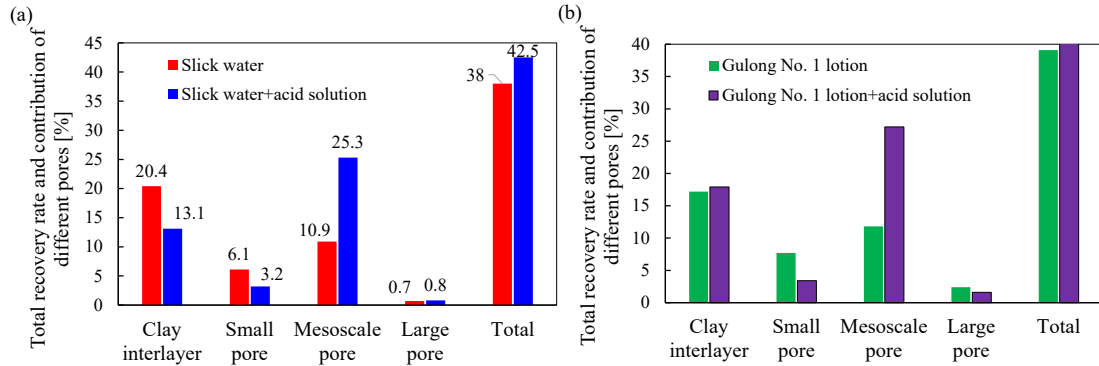
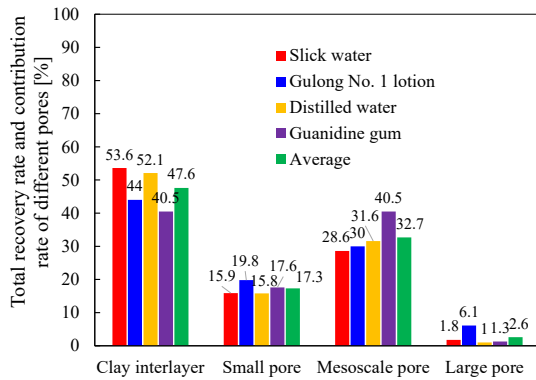
3.1.2 Laminated shale

The recovery rates of rich bedding shale under different injection media conditions calculated based on NMR testing results are shown in Table 2 and Fig. 2.

From Table 2 and Fig. 2, it can be found that: (a) The total recovery rate of single agent imbibition is in the order of GJ surfactant (39.1%) > slick water (38.0%) > guanidine gum (34.7%) > distilled water (29.2%); (b) the synergistic effect of slick water and acid solution improves the imbibition efficiency of slick water by 4.52% in the order of slick water + acid solution (42.52%) > slick water (38.0%); (c) the synergistic effect of GJ surfactant and acid improves GJ imbibition recovery rate by 11.05% in the order of GJ surfa-

Table 2. Recovery rates of laminated shale under different injection media conditions.

No.	Injected medium	Length (cm)	Diameter (cm)	Dry core sample mass (g)	Saturated oil mass (g)	Saturated oil porosity (%)	Recovery rate (%)
2-2-8	Slick water	4.27	2.5	50.3448	1.453	8.61	38.02
1-19-4-1	Guanidine gum	4.14	2.48	47.5719	1.7099	10.61	34.71
1-18-5	Distilled water	4.27	2.5	50.6061	1.3319	7.89	29.23
4-13-1	GJ surfactant	6.05	2.5	70.8645	2.0203	8.45	39.12
1-12-3	Slick water + acid solution	6.54	2.50	77.9873	2.5465	9.85	42.52
1-18-4	GJ surfactant + acid solution	4.16	2.49	49.4377	1.4241	8.73	50.15

**Fig. 2.** Relationship between recovery rate/contribution rate and different pores under different injection conditions: (a) Slick water and (b) GJ surfactant.**Fig. 3.** Total recovery and contribution of different pore scales.

ctant + acid solution (50.15%) > GJ surfactant (39.1%); (d) the enhanced oil recovery of slick water is more significant in the clay interlayer and small pores, while its ability to enhance oil recovery in mesoscale and macroscale pores is lower than that of slick water + acid solution. For the overall increase in recovery capacity, the combination of slick water + acid solution is more effective than slick water alone.

3.2 Effect of pore scale on imbibition rate

From Fig. 3, it can be found that the effect of pore scale is in the order of interlayer clay (47.6%) > mesoscale pores (32.7%) > small pores (17.3%) > large pores (2.6%). Secondly, under different pore size conditions, the enhanced oil recovery ability of different external fluids varies. Therefore, for shale oil reservoirs with different pore characteristics, to improve the

recovery efficiency, different external fluids can be selected to enhance oil recovery; for reservoirs with developed clay interlayer pores, slick water can be used as much as possible; for reservoirs with small pore development, Gulong No. 1 lotion is recommended; for shale oil with developed mesoscale pores, guanidine gum can be commonly used; for shale oil reservoirs with large pore development, Gulong No. 1 lotion can be commonly used.

3.3 Analysis of NMR test results

3.3.1 Guanidine gum imbibition results

The results of guanidine gum imbibition in core 4-10-7 are shown in Table 3, Figs. 4 and 5. From these data, it can be found that the total recovery rate of guanidine gum in core 4-10-7 is 30.38%, with clay interlayer, small pore, medium pore, and large pore being 7.05%, 5.61%, 16.27%, and 1.45%. The guanidine gum imbibition is 32.55%. Among them, the average values of clay interlayer and small/medium/large pores are 10.56%, 5.87%, 15.17%, and 0.96%.

It can be seen from Figs. 4 and 5 that the core samples treated with guanidine gum have the highest increase in saturated oil between clay layers, accounting for 52.08%. The increment of saturated oil in macroscale pores is the smallest, accounting for only 6.15%, which is 45.93% less than that of saturated oil between clay layers. The proportion of oil produced by imbibition in the mesoscale pore is the highest. On the other hand, the recovery rate of small pores is the highest, reaching 79.49%. The porosity recovery rate between

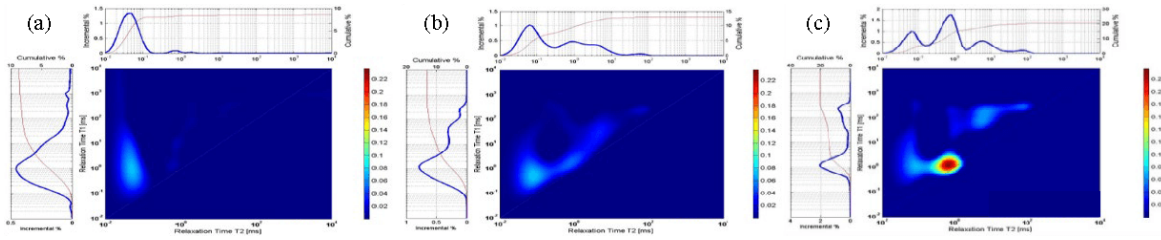


Fig. 4. NMR testing results of shale core for different states of core 4-10-7: (a) Dry sample, (b) saturated oil and (c) guanidine gum imbibition.

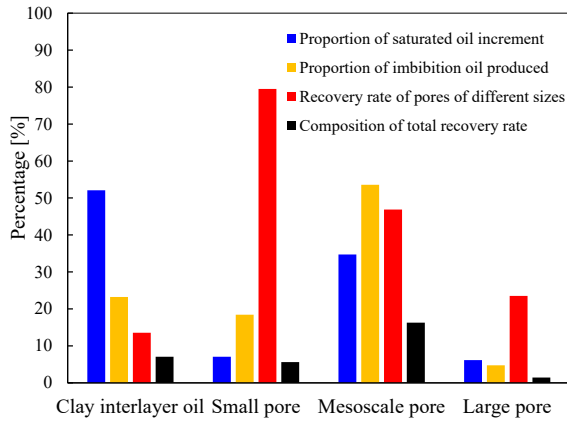


Fig. 5. Interpretation data of guanidine gum imbibition in core 4-10-7.

clay layers is the lowest at only 13.54%. Among the components of total recovery rate, mesoscale pores have the highest proportion, while macroscale pores have the lowest total recovery rate at only 1.05%.

The results of guanidine gum imbibition in core 1-19-4-1 are presented in Table 3 and Fig. 6. From these data, it can be found that the total recovery rate is 34.71%. Among them, those of the clay interlayer and small/mesoscale/macroscale pores are 14.07 %, 6.12 %, 14.07 %, and 0.46 %, respectively.

3.3.2 Distilled/slick water imbibition results

The results of distilled water imbibition in core 2-2-4 are shown in Table 3, Figs. 7 and 8. From these data, it can be found that, firstly, the total oil recovery rate of core 2-2-4 by distilled water imbibition is 32.92%. Among them, those of the clay interlayer and small/mesoscale/large pores are 19.15%, 3.86%, 9.09%, and 0.83%. Secondly, the average total recovery rate of distilled water imbibition is 31.08%. The average values of clay interlayer, small pores, mesoscale pores, and macroscale pores are 17.20%, 4.22%, 9.16%, and 0.56%, respectively.

From Figs. 7 and 8, it can be seen that, firstly, the saturated oil increment between clay layers is the highest in the core samples treated with distilled water. The lowest proportion of macroscale pores is 66.94%, which is 62.12% higher than that of macroscale pores. Oil production through imbibition between clay layers is also the highest, accounting for 58.16%, which is 55.65% higher than that by imbibition and extraction through large pores. The pore recovery rate of small pores is 68.29%, accounting for the highest proportion. Secondly, the

porosity recovery rate of mesoscale pores is 40.24%, while the proportion of large pores is the lowest at only 17.14%. The proportion of interlayer clay in the total recovery rate is the highest, whereas the contribution of macroscale pores to the total recovery rate is only 0.83%.

The results of distilled water imbibition in core 1-18-5 are presented in Table 3 and Fig. 9. From these data, it can be found that total recovery rate of core 1-18-5 by distilled water imbibition is 29.23%. Among them, those of the clay interlayer and small/mesoscale/macroscale pores are 15.24%, 4.62%, 9.23%, 0.28%.

The results of slick water imbibition in core 2-2-8 are shown in Table 4 and Fig. 10. From these data, it can be found that total recovery rate of 2-8 # core is 38.02%, with those of clay interlayer, small pore, medium pore, and large pores being 20.39%, 6.06%, 10.88%, and 0.69%, respectively.

3.3.3 GJ surfactant imbibition results

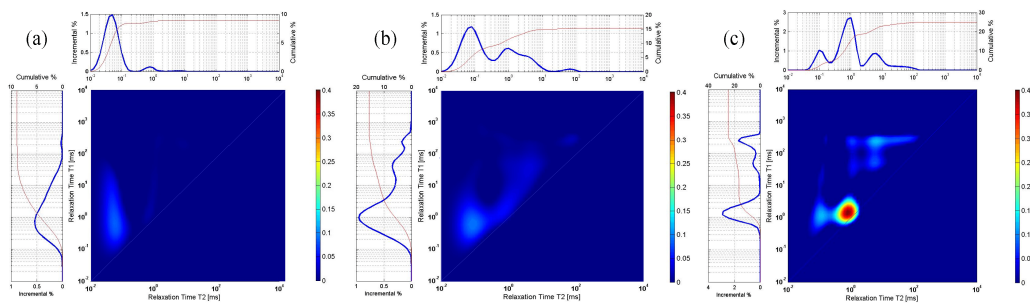
The results of GJ surfactant imbibition in core 2-3-1 are presented in Table 4, Figs. 11 and 12. From these data, it can be found that the total recovery rate of GJ surfactant imbibition in core 2-3-1 is 39.79%. Among them, those of the clay interlayer and small/mesoscale/large pores are 14.56%, 2.84%, 19.72%, and 2.66%, respectively. The average total oil recovery rate of GJ surfactant imbibition is 39.46%. Among them, the average values of clay interlayer, small pore, medium pore, and large pore are 15.86%, 5.29%, 15.74%, and 2.53%, respectively.

It can be seen from Figs. 11 and 12 that the core samples treated with GJ surfactant shows the highest increase in saturated oil between clay layers, accounting for 56.84%. Oil saturation in the smallest pores is 52.75% lower than that in the interlayer of clay. The highest oil production is achieved through imbibition and extraction in the middle pores, accounting for 49.55%, which is 42.85% higher than the oil production through imbibition and extraction in the large pores. The pore recovery rate of small pores is 69.57%, accounting for the highest proportion. Secondly, the porosity recovery rate of mesoscale pores is 62.36% and the proportion of interlayer clay is the lowest at only 25.63%. The mesoscale pores have the highest overall recovery rate, accounting for 19.72%. Meanwhile, large pores only account for 2.66% of the total recovery rate, 17.06% lower than the mesoscale pore.

The results of GJ surfactant imbibition in core 4-13-1 are shown in Table 4 and Fig. 13. From these data, it can be found that the total recovery rate of GJ surfactant imbibition in core

Table 3. Interpretation of NMR testing results of core 1-10-7, 1-19-4-1, 2-2-4 and 1-18-5.

No.	Status	Clay interlayer oil	Small pore oil	Mesoscale pore oil	Large pore oil	Accumulated oil signal quantity
4-10-7	Dry sample	0.2	0.07	0.08	0.07	0.42
	Signal quantity of fluid after saturated oil	3.08	0.46	2	0.41	5.95
	Fluid signal quantity after imbibition	2.69	0.15	1.1	0.33	4.27
	Proportion of saturated oil increment	52.08	7.05	34.72	6.15	100
	Proportion of imbibition oil produced	23.21	18.45	53.57	4.76	100.00
	Recovery rate of pores of different sizes	13.54	79.49	46.88	23.53	30.38
	Contribution to total recovery rate	7.05	5.61	16.27	1.45	30.38
1-19-4-1	Dry sample	0.28	0.13	0.05	0	0.46
	Signal quantity of fluid after saturated oil	3.48	1.1	2.13	0.29	7
	Fluid signal quantity after imbibition	2.56	0.7	1.21	0.26	4.73
	Proportion of saturated oil increment	48.93	14.83	31.8	4.43	100
	Proportion of oil produced by imbibition	40.53	17.62	40.53	1.32	100
	Recovery rate of pores of different sizes	28.75	41.24	44.23	10.34	34.71
	Contribution to total recovery rate	14.07	6.12	14.07	0.46	34.71
2-2-4	Dry sample	0.24	0.14	0.05	0	0.43
	Signal quantity of fluid after saturated oil	5.1	0.55	1.69	0.35	7.69
	Fluid signal quantity after imbibition	3.71	0.27	1.03	0.29	5.3
	Proportion of saturated oil increment	66.94	5.65	22.59	4.82	100
	Proportion of imbibition oil produced	58.16	11.72	27.62	2.51	100.00
	Recovery rate of pores of different sizes	28.60	68.29	40.24	17.14	32.92
1-18-5	Dry sample	0.54	0.08	0.08	0.03	0.73
	Signal quantity of fluid after saturated oil	5.28	0.53	1.86	0.21	7.88
	Fluid signal quantity after imbibition	4.19	0.2	1.2	0.2	5.79
	Proportion of saturated oil increment	66.26	6.33	24.78	2.63	100
	Proportion of oil produced by imbibition	52.15	15.79	31.58	0.96	100
	Recovery rates of pores of different sizes	23.00	73.33	37.08	11.11	29.23
	Contribution to total recovery rate	15.24	4.62	9.23	0.28	29.23

**Fig. 6.** Testing data of 1-19-4-1 after guanidine gum imbibition: (a) Dry sample, (b) saturated oil and (c) guanidine gum imbibition.

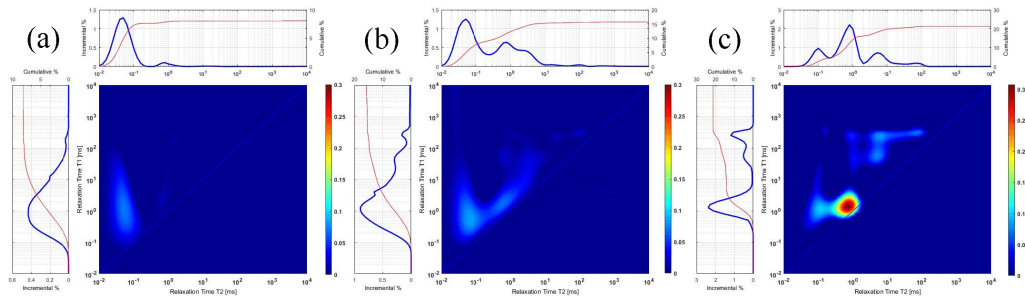


Fig. 7. NMR testing results of shale core 2-2-4 for different states: (a) Dry sample, (b) saturated oil and (c) distilled water imbibition.

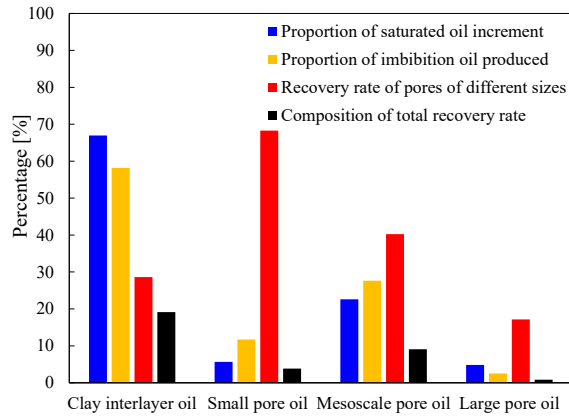


Fig. 8. Interpretation data of distilled water imbibition in core 2-2-4.

4-13-1 is 39.12%. Among them, those of the clay interlayer and small/mesoscale/macroscale pores are 17.22 %, 7.74 %, 11.75 %, 2.40 %.

3.3.4 Alkali solution imbibition results

The results of alkali solution imbibition in core 4-11-6 are shown in Table 4, Figs. 14 and 15. From these data, it can be found that, firstly, total recovery rate of alkaline imbibition in core 4-11-6 is 61.50%, among which those of the clay interlayer and small/medium/large pore are 20.93%, 2.71%, 37.20%, 0.65%. Secondly, the average total recovery rate of alkali solution imbibition is 55.48%. Among them, the average values of clay interlayer, small pores, mesoscale pores, and macroscale pores are 22.60%, 2.84%, 29.24%, and 0.80%, respectively.

From Figs. 14 and 15, it can be found that, firstly, the core samples treated with alkaline solution have the highest percentage of saturated oil increment in the mesoscale pores and the highest percentage of oil extracted through imbibition, which are 56.83% and 60.49%, respectively. Secondly, the pore recovery rate of small pores also reaches 92.59%. The recovery rate of interlayer pores is lowest in clay at only 52.88%. Regarding the contribution to the total recovery rate, mesoscale pores have the highest proportion, accounting for 37.20%. Meanwhile, the contribution of large pores to the total recovery rate is only 0.65%, which is 36.55% lower than that of mesoscale pores.

3.3.5 Acid solution imbibition results

The results of acid solution imbibition in core 1-17-6 are presented in Table 5, Figs. 16 and 17. From these data, it can be found that, firstly, the total recovery rate of acid imbibition in core 1-17-6 is 60.92%. Among them, the contribution of the clay interlayer and small/mesoscale/macroscale pores are 8.68%, 39.95%, 11.79%, 0.50%. Secondly, the average total recovery rate of acid imbibition is 53.92%. Among them, the average values of clay interlayer and small/mesoscale/large pores are 9.56%, 22.67%, 21.12%, 0.58%.

It can be seen from Figs. 16 and 17 that after acid treatment, the saturated oil increment in small pores is the highest, accounting for 58.93%. That of the largest pore is the lowest at only 0.99%, which is 57.94% lower than the small pore. Moreover, the imbibition from small pores is also the highest, accounting for 65.58%. Oil production through imbibition from large pores is 0.81%, while that from small pores is 64.77% higher. The pore recovery rate of small pores is 67.79%, accounting for the highest proportion. Secondly, the porosity recovery rate of mesoscale pores is 64.63%, with the lowest proportion of interlayer clay. The total recovery rate is highest for small and mesoscale pores, accounting for 39.95% of the total recovery rate, while the contribution of large pores to the total recovery rate is only 0.5%.

The results of GJ and acid composite imbibition in core 1-18-4 are presented in Table 5 and Fig. 18. From these data, it can be found that the total recovery rate of core 1-18-4 through the imbibition of GJ and acid composite is 50.15%. Among them, the interlayer and small to macroscale pores of clay are 17.86%, 3.42%, 27.23%, 1.64%.

The results of slick water and acid composite imbibition in core 1-12-3 are shown in Table 5 and Fig. 19. From these data, it can be found that the total recovery rate of core 1-12-3 through the imbibition of composite of slick water and acid solution is 42.52%. Among them, the clay interlayer, small to macroscale pores are 13.11%, 3.18%, 25.30%, 0.79%.

4. Conclusions

In this paper, the contribution of pore scales with varying injection media to the recovery rate of imbibition has been quantified. The key findings are shown below:

- 1) The average contribution rate of different types of pores was in the order of interlayer clay (47.6%) > mesoscale

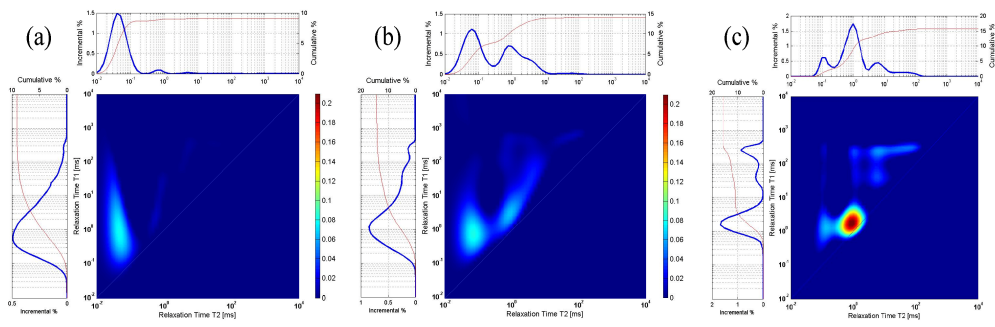


Fig. 9. NMR testing results of shale core1-18-5 for different states: (a) Dry sample, (b) saturated oil and (c) after distilled water imbibition.

Table 4. Interpretation of NMR testing results of core 2-2-8, 2-3-1, 4-13-1 and 4-11-6.

No.	Status	Clay interlayer oil	Small pore oil	Mesoscale pore oil	Large pore oil	Accumulated oil signal quantity
2-2-8	Dry sample	0.39	0.07	0.09	0.04	0.59
	Signal quantity of fluid after saturated oil	5.15	0.54	1.84	0.32	7.85
	Fluid signal quantity after imbibition	3.67	0.1	1.05	0.27	5.09
	Proportion of saturated oil increment	65.56	6.47	24.1	3.86	100
	Proportion of oil produced by imbibition	53.62	15.94	28.62	1.81	100
	Recovery rate of pores of different sizes	31.09	93.62	45.14	17.86	38.02
	Contribution to total recovery rate	20.39	6.06	10.88	0.69	38.02
2-3-1	Dry sample	0.27	0.09	0.07	0.06	0.49
	Signal quantity of fluid after saturated oil	3.47	0.32	1.85	0.48	6.12
	Fluid signal quantity after imbibition	2.65	0.16	0.74	0.33	3.88
	Proportion of saturated oil increment	56.84	4.09	31.62	7.46	100
	Proportion of imbibition oil produced	36.61	7.14	49.55	6.70	100
	Recovery rate of pores of different sizes	25.63	69.57	62.36	35.71	39.79
	Contribution to total recovery rate	14.56	2.84	19.72	2.66	39.79
4-13-1	Dry sample	0.21	0.15	0.07	0	0.43
	Signal quantity of fluid after saturated oil	4.37	0.97	2.4	0.18	7.92
	Fluid signal quantity after imbibition	3.08	0.39	1.52	0	4.99
	Proportion of saturated oil increment	55.54	10.95	31.11	2.40	100
	Proportion of oil produced by imbibition	44.03	19.80	30.03	6.14	100
	Recovery rate of pores of different sizes	31.01	70.73	37.77	100	39.12
	Contribution to total recovery rate	17.22	7.74	11.75	2.40	39.12
4-11-6	Dry sample	0.49	0.13	0.06	0	0.68
	Signal quantity of fluid after saturated oil	4.14	0.4	5.3	0.06	9.9
	Fluid signal quantity after imbibition	2.21	0.15	1.87	0	4.23
	Proportion of saturated oil increment	39.59	2.93	56.83	0.65	100
	Proportion of imbibition oil produced	34.04	4.41	60.49	1.06	100
	Recovery rate of pores of different sizes	52.88	92.59	65.46	100	61.50
	Contribution to total recovery rate	20.93	2.71	37.20	0.65	61.50

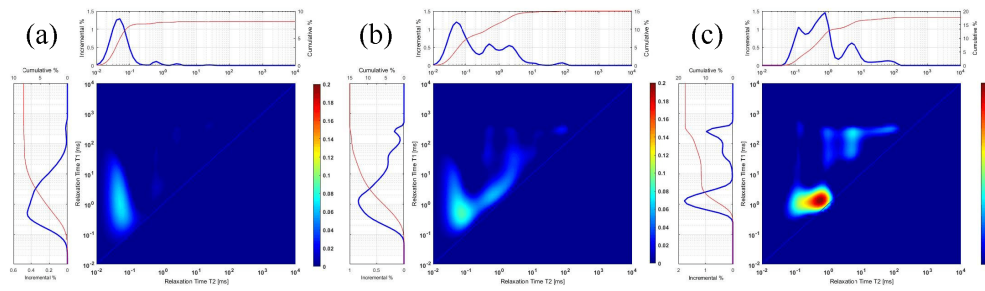


Fig. 10. NMR testing results of shale core 2-2-8 after slick water imbibition: (a) Dry sample, (b) saturated oil and (c) after slick water imbibition.

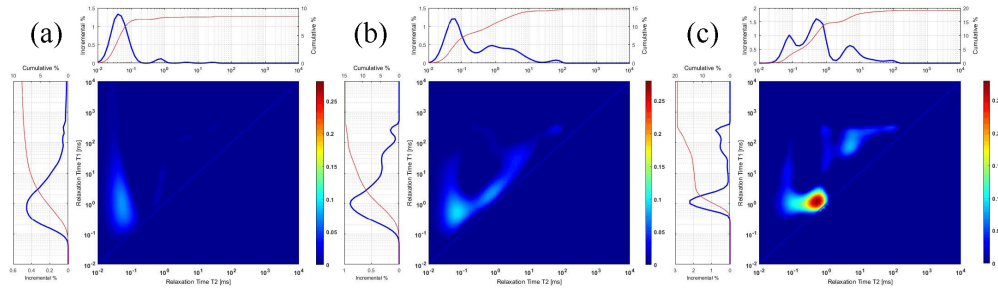


Fig. 11. NMR testing results of shale core for different states of core 2-3-1: (a) Dry sample, (b) saturated oil and (c) GJ surfactant imbibition.

pores (32.7%) > small pores (17.3%) > large pores (2.6%).

- 2) The total imbibition recovery of shale with millimeter-scale sandy laminae was ranked as alkali solution (61.50%) > acid solution (60.92%) > GJ surfactant (39.79%) > distilled water (32.92%) > guanidine gum (30.38%).
- 3) The total imbibition recovery of laminated shale was ranked as GJ surfactant (39.1%) > slick water (38.0%) > guanidine gum (34.7%) > distilled water (29.2%).

Acknowledgements

This research was funded by the Heilongjiang “Open Competition” projects (Nos. 2023ZXJ06A02 and DQYT 2022-JS-757).

Supplementary file

<https://doi.org/10.46690/capi.2025.04.03>

Conflict of interest

The authors declare no competing interest.

Open Access This article is distributed under the terms and conditions of the Creative Commons Attribution (CC BY-NC-ND) license, which permits unrestricted use, distribution, and reproduction in any medium, provided the original work is properly cited.

References

Chen, X., Zhu, J., Chao, L., et al. Investigation of effect and mechanism of active water and CO₂ huff-and-puff on enhanced oil recovery in tight reservoirs. *Capillarity*, 2025, 14(1): 23-34.

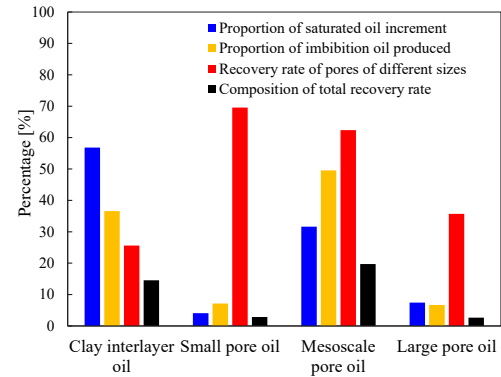


Fig. 12. Interpretation data of GJ surfactant imbibition in core 2-3-1.

Faramarzi, M., Tabatabaei, S. M., Sedae, B., et al. Saturation-functions models in CO₂-brine system: A comparative study. *Capillarity*, 2025, 14(2): 35-52.

Gao, X., Yang, S., Tian, L., et al. System and multi-physics coupling model of liquid-CO₂ injection on CO₂ storage with enhanced gas recovery (CSEGR) framework. *Energy*, 2024, 294: 130951.

Gao, X., Yang, S., Wang, B., et al. Wellbore-reservoir and multiphysics coupling model for liquid CO₂ cyclic injection in a CCUS-EGR framework. *Journal of Hydrology*, 2025a, 658: 133188.

Gao, X., Yang, S., Wang, B., et al. Pore-scale modeling of multiple fluids flow transport kinetics for CO₂ enhanced gas recovery. *Energy*, 2025b, 315, 134486.

Jiang, Y., Liu, H., Chai, C., et al. Logging evaluation of shale oil in Jiyang Depression. *Petroleum Geology and Recovery Efficiency*, 2023, 30(1): 21-34.

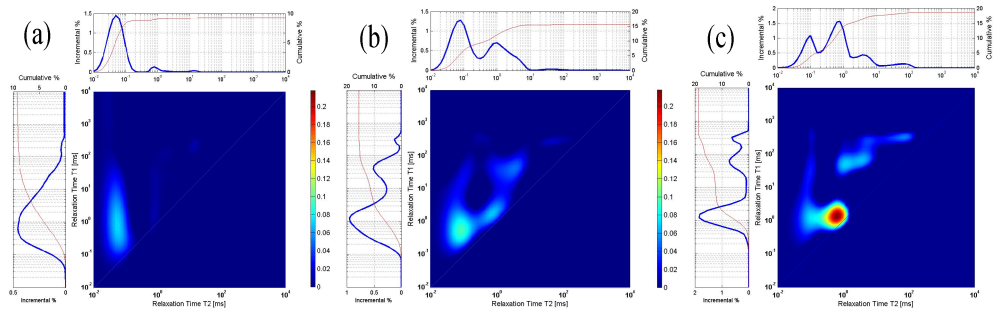


Fig. 13. NMR testing results of shale core 4-13-1 for different states: (a) Dry sample, (b) saturated oil and (c) GJ surfactant imbibition.

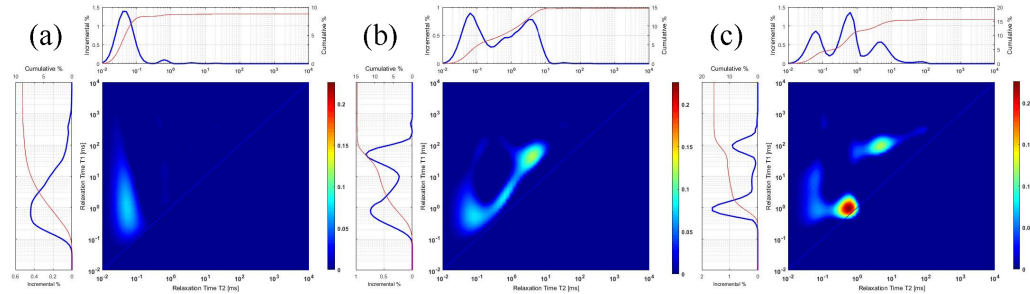


Fig. 14. NMR testing results of shale core 4-11-6 for different states: (a) Dry sample, (b) saturated oil and (c) alkali solution imbibition.

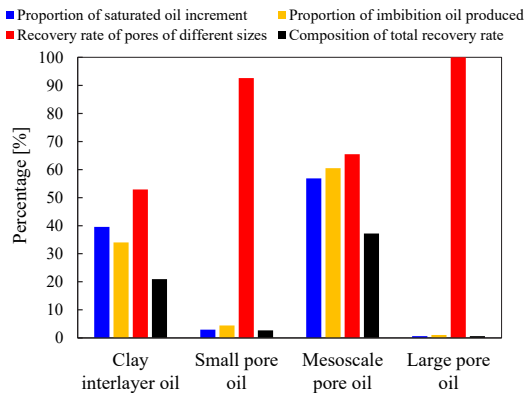


Fig. 15. Interpretation data of alkali solution imbibition in core 4-11-6.

Lee, J. H., Jeong, M. S., Lee, K. S. Comprehensive modeling of CO₂ Huff-n-Puff in asphaltene-damaged shale reservoir with aqueous solubility and nano-confinement. *Journal of Industrial and Engineering Chemistry*, 2020, 90: 232-243.

Liu, B., Song, Y., Zhu, K., et al. Mineralogy and element geochemistry of salinized lacustrine organic-rich shale in the Middle Permian Santanghu Basin: Implications for paleoenvironment, provenance, tectonic setting and shale oil potential. *Marine and Petroleum Geology*, 2020a, 120: 104569.

Liu, B., Sun, J., Zhang, Y., et al. Reservoir space and enrichment model of shale oil in the first member of Cretaceous Qingshankou Formation in the Changling sag, southern Songliao Basin, NE China. *Petroleum Exploration and*

Development, 2021, 48(3): 608-624.

Liu, B., Wang, H., Fu, X., et al. Lithofacies and depositional setting of a highly prospective lacustrine shale oil succession from the Upper Cretaceous Qingshankou Formation in the Gulong Sag, northern Songliao Basin, Northeast China. *AAPG Bulletin*, 2019, 103: 405-432.

Liu, B., Yang, Y., Li, J., et al. Stress sensitivity of tight reservoirs and its effect on oil saturation: A case study of Lower Cretaceous tight clastic reservoirs in the Hailar Basin, Northeast China. *Journal of Petroleum Science and Engineering*, 2020b, 184, 106484.

Liu, H., Huang, Y., Cai, M., et al. Practice and development suggestions for hydraulic fracturing technology in the Gulong shale oil reservoirs in Songliao Basin, NE China. *Petroleum Exploration and Development*, 2023a, 50(3): 603-612.

Liu, H., Kuang, L., Li, G., et al. Considerations and suggestions on optimizing completion methods of continental shale oil in China. *Acta Petrolei Sinica*, 2020c, 41(4): 489-496.

Liu, H., Meng, S., Wang, S. L., et al. Mechanical characteristics and fracture propagation mechanism of the Gulong shale. *Oil & Gas Geology*, 2023b, 44(4): 820-828.

Liu, X., Meng, S., Liang, Z., et al. Microscale crack propagation in shale samples using focused ion beam scanning electron microscopy and three-dimensional numerical modeling. *Petroleum Science*, 2023c, 20(3): 1488-1512.

Lu, Z., Zeng, C., Zhang, Y., et al. Study of the pore size influence on infiltration of porous media considering capillary effect. *Capillarity*, 2025, 14(1): 1-12.

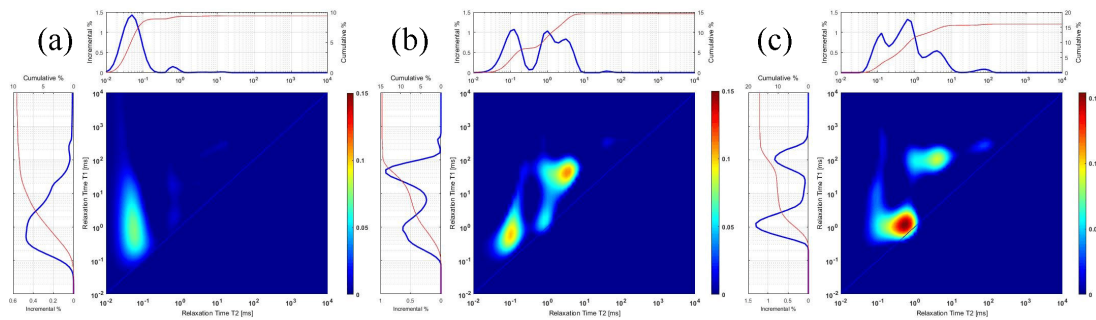


Fig. 16. NMR testing results of shale core for different states of core 1-17-6: (a) Dry sample, (b) saturated oil and (c) acid solution imbibition.

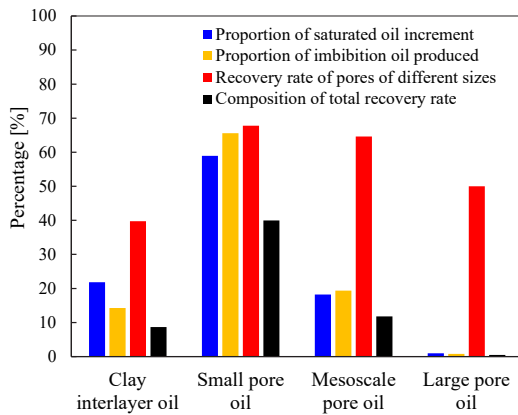


Fig. 17. Interpretation data of acid solution imbibition in core 1-17-6.

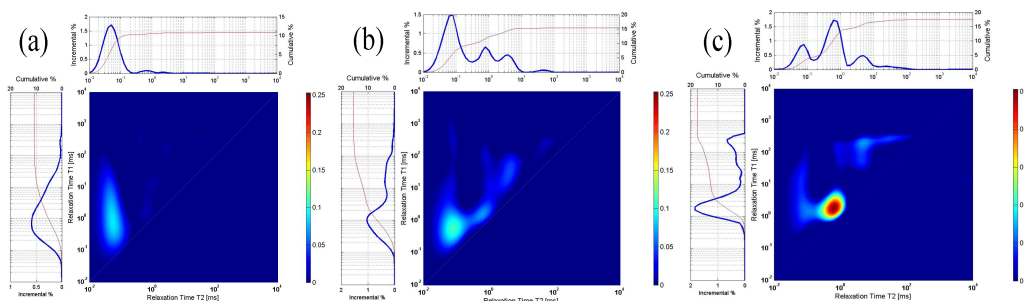
- Ma, L., Doney, P. J., Rutter, E., et al. A novel upscaling procedure for characterizing heterogeneous shale porosity from nanometer-to millimetre-scale in 3D. *Energy*, 2019, 181: 1285-1297.
- Maghzi, A., Mohammadi, S., Ghazanfari, M. H., et al. Monitoring wettability alteration by silica nanoparticles during water flooding to heavy oils in five-spot systems: A pore-level investigation. *Experimental Thermal and Fluid Science*, 2012, 40: 168-176.
- Meng, S., Li, D., Liu, X., et al. Study on dynamic fracture growth mechanism of continental shale under compression failure. *Gas Science and Engineering*, 2023a, 114: 2949-9089.
- Meng, S., Zhang, Z., Tao, J., et al. A novel upscaling method for evaluating mechanical properties of the shale oil reservoir based on cluster analysis and nanoindentation. *Journal of Energy Resources Technology*, 2023b, 145(11): 112901.
- Mohagheghian, E., Hassanzadeh, H., Chen, Z. Evaluation of shale-gas-phase behavior under nanoconfinement in multi-mechanistic flow. *Industrial & Engineering Chemistry Research*, 2020, 59(33): 15048-15057.
- Naveen, P., Asif, M., Ojha, K. Integrated fractal description of nanopore structure and its effect on CH₄ adsorption on Jharia coals, India. *Fuel*, 2018, 232: 190-204.
- Ratnakar, R. R., Dindoruk, B. A New technique for simultaneous measurement of nanodarcy-range permeability

and adsorption isotherms of tight rocks using magnetic suspension balance. *SPE Journal*, 2019, 24(6): 2482-2503.

- Roslin, A., Pokrajac, D., Wu, K., et al. 3D pore system reconstruction using nano-scale 2D SEM images and pore size distribution analysis for intermediate rank coal matrix. *Fuel*, 2020, 275: 117934.
- Saghandal, F., Salehi, M. B., Taghikhani, V. Hydrogel nanocomposite network elasticity parameters as a function of swelling ratio: From micro to macro flooding. *Journal of Industrial and Engineering Chemistry*, 2023, 125: 163-177.
- Sakurovs, R., Koval, L., Grigore, M., et al. Nanometre-sized pores in coal: Variations between coal basins and coal origin. *International Journal of Coal Geology*, 2018, 186: 126-134.
- Shelare, S. D., Belkhode, P. N., Nikam, K. C., et al. Biofuels for a sustainable future: Examining the role of nano-additives, economics, policy, internet of things, artificial intelligence and machine learning technology in biodiesel production. *Energy*, 2023, 282: 128874.
- Sun, F., Liu, D., Cai, Y., et al. Coal rank-pressure coupling control mechanism on gas adsorption/desorption in coalbed methane reservoirs. *Energy*, 2023, 270: 126849.
- Sun, F., Yao, Y., Chen, M., et al. Performance analysis of superheated steam injection for heavy oil recovery and modeling of wellbore heat efficiency. *Energy*, 2017, 125: 795-804.
- Sun, F., Yao, Y., Li, X. The Heat and Mass Transfer Characteristics of Superheated Steam Coupled with Non-condensing Gases in Horizontal Wells with Multi-point Injection Technique. *Energy*, 2018, 143: 995-1005.
- Tang, X., Jiang, Z., Jiang, S., et al. Heterogeneous nanoporosity of the Silurian Longmaxi Formation shale gas reservoir in the Sichuan Basin using the QEMSCAN, FIB-SEM, and nano-CT methods. *Marine and Petroleum Geology*, 2016, 78: 99-109.
- Tao, J., Meng, S., Li, D., et al. Analysis of CO₂ effects on porosity and permeability of shale reservoirs under different water content conditions. *Geoenergy Science and Engineering*, 2023, 226: 2949-8910.
- Wang, Q., Hu, Q., Zhao, C., et al. Micro- to nano-scale areal heterogeneity in pore structure and mineral compositions

Table 5. Interpretation of NMR testing results of core 1-17-6, 1-18-4 and 1-12-3.

No.	Status	Clay interlayer oil	Small pore oil	Mesoscale pore oil	Large pore oil	Accumulated oil signal quantity
1-17-6	Dry sample	0.23	0.22	0.09	0	0.54
	Signal quantity of fluid after saturated oil	1.99	4.97	1.56	0.08	8.6
	Fluid signal quantity after imbibition	1.29	1.75	0.61	0.04	3.69
	Proportion of saturated oil increment	21.84	58.93	18.24	0.99	100
	Proportion of imbibition oil produced	14.26	65.58	19.35	0.81	100
	Recovery rate of pores of different sizes	39.77	67.79	64.63	50.00	60.92
	Contribution to total recovery rate	8.68	39.95	11.79	0.50	60.92
1-18-4	Dry sample	0.83	0.1	0.13	0.05	1.11
	Signal quantity of fluid after saturated oil	4.12	0.52	2.97	0.22	7.83
	Fluid signal quantity after imbibition	2.92	0.29	1.14	0.11	4.46
	Proportion of saturated oil increment	49.01	6.26	42.24	2.49	100
	Proportion of oil produced by imbibition	35.61	6.82	54.30	3.26	100
	Recovery rate of pores of different sizes	36.47	54.76	64.44	64.71	50.15
	Contribution to total recovery rate	17.86	3.42	27.23	1.64	50.15
1-12-3	Dry sample	0.2	0.07	0.07	0	0.35
	Signal quantity of fluid after saturated oil	3.79	0.44	3.48	0.18	7.9
	Fluid signal quantity after imbibition	2.8	0.2	1.57	0.12	4.69
	Proportion of saturated oil increment	47.55	4.92	45.12	2.41	100
	Proportion of oil produced by imbibition	30.84	7.48	59.50	1.87	100
	Recovery rate of pores of different sizes	27.58	64.86	56.01	33.33	42.52
	Contribution to total recovery rate	13.11	3.18	25.30	0.79	42.52

**Fig. 18.** NMR testing results of shale core 1-18-4 imbibition: (a) Dry sample, (b) saturated oil and (c) GJ and acid composite.

of a sub-decimeter-sized Eagle Ford Shale. *International Journal of Coal Geology*, 2022, 261: 104093.

Wang, L., Wang, H., Xia, X., et al. The effects of clay minerals on imbibition in shale reservoirs: A review. *Capillarity*, 2025, 14(1): 13-22.

Wei, J., Shang, D., Zhao, X., et al. Experimental study on production characteristics and enhanced oil recovery during imbibition and huff-n-puff injection in shale reservoir. *Capillarity*, 2024, 12(2): 41-56.

Xiang, Z., Hu, Z., Cao, D., et al. Metal-organic frameworks with incorporated carbon nanotubes: Improving

carbon dioxide and methane storage capacities by lithium doping. *Angewandte Chemie-International Edition*, 2011, 50(2): 491-494.

Xiao, W., Ren, J., Wang, L., et al. Experimental study on oil production characteristics in shale oil from Xi233 area Chang7 reservoir during injecting associated gas. *Petroleum Geology and Recovery Efficiency*, 2022, 29(5): 91-101.

Xu, H., Zhao, D. Research on brittleness evaluation of deep shale reservoirs and optimization approach of comprehensive brittleness index evaluation: A case study of

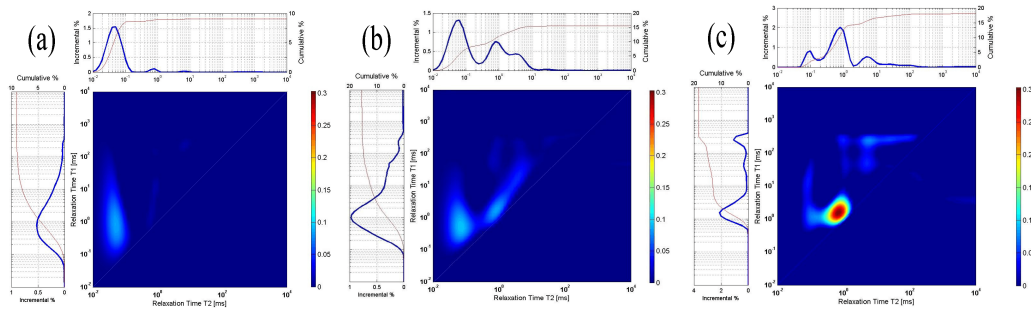


Fig. 19. NMR testing results of shale core 1-12-3 imbibition: (a) Dry sample, (b) saturated oil and (c) slick water and acid composite solution imbibition.

Wufeng-Longmaxi Formation from well Z-3. *Unconventional Oil & Gas*, 2023, 10(1): 84-92.

- Yakasai, F., Jaafar, M. Z., Bandyopadhyay, S., et al. Current developments and future outlook in nanofluid flooding: A comprehensive review of various parameters influencing oil recovery mechanisms. *Journal of Industrial and Engineering Chemistry*, 2021, 93: 138-162.
- Yang, X., Cai, J., Jiang, G., et al. Modeling of nanoparticle fluid microscopic plugging effect on horizontal and vertical wellbore of shale gas. *Energy*, 2022, 239(Part B): 122130.
- Yu, H., Xu, W., Li, B., et al. Hydraulic fracturing and enhanced recovery in shale reservoirs: Theoretical analysis to engineering applications. *Energy & Fuels*, 2023, 37(14): 9956-9997.
- Yuan, B., Zhao, Z., Meng, S., et al. Intelligent identification and real-time warning method of diverse complex events in horizontal well fracturing. *Petroleum Exploration and Development*, 2023, 50(6): 1487-1496.
- Zhang, J., Tang, Y., He, D., et al. Full-scale nanopore system and fractal characteristics of clay-rich lacustrine shale combining FE-SEM, nano-CT, gas adsorption and mercury intrusion porosimetry. *Applied Clay Science*, 2020, 196: 105758.
- Zhang, M., Liu, Z., Pan, B., et al. Molecular simulation on CO₂/H₂S co-adsorption in organic and inorganic shale nanopores. *Applied Surface Science*, 2023a, 624: 157167.
- Zhang, T., Dong, M., An, J., et al. Oil and gas enrichment characteristics and main controlling factors of Chang7 shale in Fuxian Area. *Unconventional Oil & Gas*, 2023b, 10(5): 75-83.
- Zhao, M., Cheng, Y., Wu, Y., et al. Enhanced oil recovery mechanism by surfactant-silica nanoparticles imbibition in ultra-low permeability reservoirs. *Journal of Molecular Liquids*, 2022, 348: 118010.
- Zheng, L., Zhao, Q., Dong, Y., et al. Molecular dynamics simulation of sub- and supercritical water extraction shale oil in slit nanopores. *The Journal of Supercritical Fluids*, 2023, 195: 105862.
- Zheng, L., Jiang, J., Xiao, W., et al. A NMR investigation of spontaneous and forced imbibition of shale under different flow and confinement conditions. *Capillarity*, 2025, 14(2): 53-62.
- Zhong, C., Qin, Q., Fan, C., et al. Effect of nanometer pore structure on methane adsorption capacity in organic-rich shale. *Petroleum Science and Technology*, 2019, 37(11): 1243-1250.
- Zhou, J., Zhang, C., Ranjith, P. G. Behaviours of methane and water in heterogeneous shale nanopores: Effect of water saturation and pore size. *Fuel*, 2023, 335: 126675.
- Zhou, S., Yan, G., Xue, H., et al. 2D and 3D nanopore characterization of gas shale in longmaxi formation based on FIB-SEM. *Marine and Petroleum Geology*, 2016, 73: 174-180.
- Zhu, H., Ju, Y., Huang, C., et al. Microcosmic gas adsorption mechanism on clay-organic nanocomposites in a marine shale. *Energy*, 2020, 197: 117256.